

Induction annealing and subsequent quenching: Effect on the thermoelectric properties of boron-doped nanographite ensembles

Ming Xie,¹ Chee Huei Lee,¹ Jiesheng Wang,¹ Yoke Khin Yap,^{1,a)} Paola Bruno,² Dieter Gruen,^{2,b)} Dileep Singh,³ and Jules Routbort⁴

¹Department of Physics, Michigan Technological University, Houghton, Michigan 49931, USA

²Materials Science Division, Argonne National Laboratory, Argonne, Illinois 60439, USA

³Nuclear Engineering Division, Argonne National Laboratory, Argonne, Illinois 60439, USA

⁴Energy Systems Division, Argonne National Laboratory, Argonne, Illinois 60439, USA

(Received 7 January 2010; accepted 12 March 2010; published online 15 April 2010)

Boron-doped nanographite ensembles (NGEs) are interesting thermoelectric nanomaterials for high temperature applications. Rapid induction annealing and quenching has been applied to boron-doped NGEs using a relatively low-cost, highly reliable, laboratory built furnace to show that substantial improvements in thermoelectric power factors can be achieved using this methodology. Details of the design and performance of this compact induction furnace as well as results of the thermoelectric measurements will be reported here. © 2010 American Institute of Physics.

[doi:10.1063/1.3378681]

I. INTRODUCTION

Thermoelectric materials are scientifically and technologically attractive because they convert heat to electricity directly without the needs of pressurized fluids and rotating machinery. It is desired to have thermoelectric materials with a high thermoelectric figure of merit Z , where $ZT = S^2 \sigma T / \kappa$. Here, S is the Seebeck coefficient, σ is electrical conductivity, κ is the thermal conductivity, and T is temperature in Kelvin.

The state-of-the-art thermoelectric conversion efficiencies are typically of the order of 10%. In order to achieve significant impacts on future global electricity generation, conversion efficiencies of 30%–40% are desired to compete with other renewable power sources such as silicon-based solar cells and solar thermal systems using electromagnetic induction technologies. In order to achieve this goal, $ZT \geq 4$ and a large temperature differential between the cold and hot ends of the thermoelectric materials is required. This ongoing quest has centered in recent years on the development of doped nanomaterials to increase thermoelectric performance.¹ It is thought that the reduced dimensionality of nanomaterials can increase phonon scattering and the density of states near the Fermi level. Based on these concepts, remarkable progress has been made, for example, ZT of ~ 2 has been obtained with nanostructured SiGe and AgPb_mSbTe_{2+m}.^{2,3} However, thermoelectric materials are heat engines, and their conversion efficiencies strongly depend on the magnitude of the temperature differential between their hot and cold junctions. To take advantage of this fact, one has to operate the hot junction continuously at tem-

peratures of about 1200 K to achieve a high Carnot efficiency. Unfortunately, very few nanomaterials preserve their nanocrystallinity under such conditions.

Owing to the high melting point of graphite (>3773 K), it is not surprising that nanographite is one of the few materials that retains its nanocrystallinity at high temperatures and is therefore a potential material for high temperature thermoelectric applications. In earlier work carried out at Argonne National Laboratory, it was recently discovered that the thermoelectric power factors of boron-doped nanographite ensembles (NGEs) increased strongly both as a function of annealing temperatures and measuring temperatures.⁴ These NGEs consist of randomly oriented nanographite without anisotropic properties. Thermoelectric power factors reached $1 \mu\text{W}/\text{K}^2 \text{cm}$ at a measuring temperature of 1200 K for samples annealed at 2500 K. Seebeck coefficients of $60 \mu\text{V}/\text{K}$ and electrical conductivities of $\sim 350 \text{ S}/\text{cm}$ were obtained for these boron-doped NGEs. The thermal conductivity obtained in those measurements was in the range of 0.03 – $0.07 \text{ W}/\text{cm K}$. From the comparison between boron-doped and undoped samples, it was concluded that boron doping substantially increases the Seebeck coefficient. Band structure calculations show that boron doping induces an acceptorlike feature near the top of the valence band of graphitic substances.^{5,6} More detailed considerations of the effects of boron doping led to the hypothesis that boron substitution in a graphite lattice introduces many configurations each one resulting in a distinct electronic state within thermal energies of the Fermi level.⁷ This supposition has now been supported by detailed density functional non-periodic cluster calculations using molecular analog models of graphene and stacked graphene sheets.⁸ Entropy transport is at the heart of thermoelectricity and our considerations provide a new approach to increasing thermoelectric performance by optimization of configurational electronic entropy.

^{a)}Electronic mail: ykyap@mtu.edu.

^{b)}Electronic mail: dmgruen@anl.gov.

Although the crucial role of boron doping in determining the thermoelectric properties of NGEs was established in the earlier studies already referred to, potential improvements in those properties due to variations in thermal treatment remain to be explored.

In order to gain a better understanding of the effect of thermal treatment on the thermoelectric properties of boron-doped NGEs, we have constructed an induction furnace to perform systematic annealing studies over a wide temperature range (1300–2400 K) under high vacuum conditions. Additionally and very importantly, induction methodology enables us rapidly to quench samples from temperatures at which diffusional processes would lead to a loss of substitutional boron if cooled slowly because of a steep gradient in boron solubility as a function of temperature.⁹ In contradistinction to a conventional graphite resistance furnace, an induction furnace by restricting heat to a small volume allows temperature reductions to occur at order of magnitude faster rates. Furthermore, induction heating saves up to about 5 h in heating time for each heat treatment cycle. Induction heating can thus be used for rapid heating and quenching of the NGEs.

Induction furnaces operating above 2300 K had been previously described.^{10–13} However, these designs are relatively old and complicated. Furthermore, the effect of quenching on thermoelectric properties has not been described previously to our knowledge. Although induction furnaces are commercially available, their designs are not flexible to accommodate different research needs in laboratories. In this article, we will describe a compact custom-built induction furnace based on an ultrahigh vacuum (UHV) chamber and standard vacuum components, which can be used for both rapid annealing and quenching. We have performed a series of annealing and quenching experiments on various NGE samples. Their effects on the Seebeck coefficients, and electrical conductivities, will be discussed here.

II. EXPERIMENTAL DETAILS

A. Design of the induction chamber

The schematic drawing and photographs of the induction chamber are shown in Figs. 1 and 2, respectively. The chamber consists of a standard UHV stainless steel four-way cross (A) with four *ConFlat* (CF) ports (two 8 in. ports at the top and the base of the chamber and two 6 in. ports at both sides). The whole chamber is wrapped by 1/4 in. diameter copper tubing for water cooling. The base of the chamber is connected to a straight reducer nipple which goes through the steel table top and is connected to a rotary pump (B) through a vacuum gauge. The left arm of the chamber is connected to an oil baffle of a *Type V70D* turbo pump (C) (*Varian*). The turbo pump operates when the base pressure in the chamber drops below 20 mtorr. The right arm of the chamber is sealed with an ac power feedthrough [(D) with a 2.75 in. flange and is connected to the copper induction coil (E) inside the chamber], which is then connected to the output of the power generator (Model SI-7KWHF, Superior Induction Co.). This generator is rated at 7 kW and operated at a maximum frequency of 400 kHz. The induction coil inside

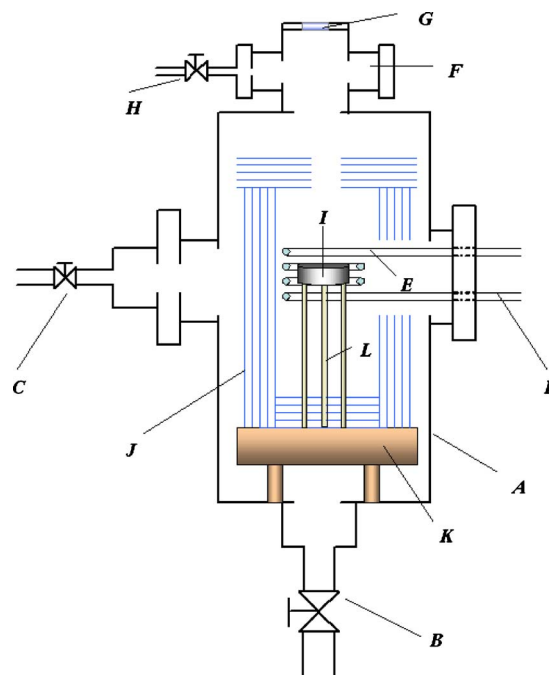


FIG. 1. (Color online) Schematic drawing of the design of the induction chamber. (A): UHV stainless steel four-way cross (8 in. in diameter), (B): rotary pump, (C): turbo pump, (D): ac power feedthrough, (E): copper induction coil, (F): UHV stainless steel four-way cross (2.5 in. in diameter), (G): silica window, (H): inlet valve for He gas, (I): graphite susceptor, (J): molybdenum radiation shields, (K): alumina disk, and (L): boron nitride rods.

the chamber is cooled by a water chiller (30 000 BTU/h with a single phase R2200V rotary vane pump by Dynaflux Co.).

The port on the top of the chamber is connected to another four-way cross [(F) with flanges of 2.5 in. in diameter]. The top arm of this smaller cross is sealed by a CF flange



FIG. 2. (Color online) (a) The exterior view and (b) the interior view of the induction chamber.

with a silica window (G). The left arm of the cross is connected to valve (H) and a helium gas tank for gas quenching purpose. The heating stage of this induction system is placed at the center of the vacuum chamber. The stage consists of a graphite susceptor (I) and the temperature of the susceptor is measured optically through the silica window by a ultrahigh performance two-color ratio fiber optic infrared pyrometer (OMEGA, Model IR-2P). This pyrometer is connected to the feedback loop of the power generator for automatic temperature control. The appearance of the overall system is shown in Fig. 2(a). The setting inside the chamber is shown in Fig. 2(b). As shown, the inner wall of the chamber and the induction copper coil are shielded by a five-layer cylindrical molybdenum radiation shield (J). This molybdenum radiation shield can reduce radiation loss to the surrounding chamber wall. An alumina plate can be seen at the center of the chamber base (K in Fig. 1). This alumina plate serves as the mechanical support for the graphite susceptor. The graphite susceptor holds NGE samples during the annealing process. This susceptor is supported by three pieces of hot-pressed boron nitride rods (L in Fig. 1, 1/4 in. in diameter, from Momentive Performance Materials) which are inserted into three holes machined at the bottom of the susceptor. The whole setting of the susceptor and boron nitride rods rests on the alumina plate.

B. Design of the susceptor and the induction coil

The surface area of a heated object in vacuum will affect the achievable maximum temperature at a particular input power since heat losses are mostly due to radiation. Although radiation losses can be reduced by employing radiation shields, an optimum design of the induction coil and the susceptor is required to achieve impedance matching between the power source and coil-susceptor.¹² Due to the dimension of our samples, we chose to have a susceptor with 1.25 in. in diameter and 0.375 in. in thickness. The induction coil (E in Fig. 1) has only two complete turns and is made of copper tubing (0.25 in. in diameter). This cylindrical coil has an inner diameter of 1.5 in. and height of 0.75 in., sufficient to produce uniform magnetic field on the whole susceptor.

The choices of the susceptor material are of prime importance for high temperature applications. For an operation temperature above 2400 K, refractory conductors such as tantalum carbide or graphite are commonly used. In this work, graphite was chosen as a susceptor material because it is relatively light in weight and easy to machine. As shown in Fig. 1, three pieces of hot-pressed boron nitride rods (L) were used to support the graphite susceptor. Boron nitride was chosen for its high stability at high temperatures and excellent electrical insulation from the base of the furnace. The alumina disk also prevents thermal conduction losses to the base of the chamber at high temperatures.

We have compared polycrystalline graphite and pyrolytic graphite (by Graphite Machining Inc.) as susceptors at 2100 K. After a series of experiments, we found that pyrolytic graphite outperformed polycrystalline graphite in many aspects. The temperature uniformity of polycrystalline graphite is poor. The temperature difference between the center and the edges of the polycrystalline graphite susceptor

can be as large as 523 K. On the other hand, pyrolytic graphite has a much more uniform temperature distribution over the area with only ~ 323 K variation under the same conditions. Polycrystalline graphite seems to have relatively poor thermal shock resistance since cracks were observed after a cumulative 20 h of heating. These cracks probably occurred during the quenching process. We did not observe cracking using a pyrolytic graphite susceptor. In fact, pyrolytic graphite was reported to survive under high temperature ramping rates of 1000 K/s without cracking.¹¹ The main disadvantages for pyrolytic graphite are the difficulty in machining and relatively high cost. Pyrolytic graphite is usually synthesized by decomposition of hydrocarbon gas limiting the thickness along the c-axis to about half an inch for most commercially available products. However, there is another issue for both polycrystalline as well as pyrolytic graphite susceptors. We found that under high vacuum, plumes appear near the surface of the susceptor near ~ 1900 K which become very noticeable at ~ 2100 K. A layer of dark coating was observed on the induction coil due to graphite evaporation after several hours of heating. This issue is moderate and did not contaminate the silica window G. This problem could probably be overcome by operating in an inert gas atmosphere. However, under such conditions, sparking between the induction coil and the chamber wall can present another category of problems which are to be avoided.¹²

C. Design of the radiation shields

In order to reduce the radiation losses from the susceptor to the vacuum chamber, the graphite susceptor is surrounded by a set of vertical radiation shields and two sets of horizontal shields, as shown in Fig. 1. Each assembly has a total of five layers of molybdenum which were fabricated from 0.05 in. thick molybdenum sheets. The vertical shields and the lower horizontal shield are both supported by the alumina plate K. The upper horizontal shield is sitting on the vertical shield. Each layer of the upper horizontal shield has a 1 in. hole which is aligned with the susceptor and the silica window to provide a clear unobstructed optical access to the susceptor for correct temperature measurements by a pyrometer.

D. Investigation of helium quenching rates

Doping of graphite by boron is a kinetic process that allows boron to diffuse into and out of graphite forming a solid solution. Quenching helps to reduce the out-diffusion of boron thus insuring that the higher boron concentrations established at higher temperatures are in fact retained at considerably lower temperatures. Gas quenching in vacuum furnaces has many advantages in comparison to oil or salt bath quenching. For example, the chamber and the samples will be free from contamination, and the quenching rate is more controllable and thus leads to a minimum heat stress and mechanical distortion. Argon, nitrogen, helium, and hydrogen are by far the most common quenching gases. Nitrogen can be very active at high temperatures and react with graphite to form cyanogens.¹² Although hydrogen has the highest thermal conductivity and provides the best cooling unifor-

TABLE I. Helium quenching rates.

Temperature of the susceptor (K)	Quenching time with helium (s)	Quenching time without helium (s)
2073—1273	~35	~55
2073—673	~160	~280

mity, safety issue is a big concern. Argon is a low-cost inert gas but it has the lowest cooling rate and cooling uniformity. We decided to choose helium gas as a compromise between high quenching rates and safety concerns. Details about gas quenching with helium can be found in the literature. Helium pressures were kept under one atmosphere and the flow rate was controlled by a mass flow controller. The quenching times with and without helium are compared and listed in Table I. The cooling rates at temperatures between 2073–1273 K are ~22.9 and ~14.5 K/s for cases with and without using helium gas, respectively. The overall cooling rates at temperatures between 2073–673 K are ~8.8 and ~5.0 K/s with and without using helium gas, respectively.

E. Reliability test of the induction furnace

We have examined the reliability of our induction furnace by continuous operation at temperatures above 2100 K up to 6 h. We did not observe any vacuum, water cooling, or electrical failures and believe to have built a quite reliable piece of equipment. We have also measured the temperature at the copper gaskets of the chamber as a function of the heating time as presented in Fig. 3. These temperatures nominally considered to be equivalent to the chamber temperature increase steadily in the first 2 h and saturate at ~425 K. The results show that the molybdenum radiation shields and water cooling jacket function properly. The maximum allowable operating temperature of the copper gaskets is around 700 K (as specified by Kurt J. Lesker Co.) which is much higher than the maximum chamber temperature which we measured. Therefore, we can conclude that our induction furnace functions reliably over prolonged periods of high temperature operation.

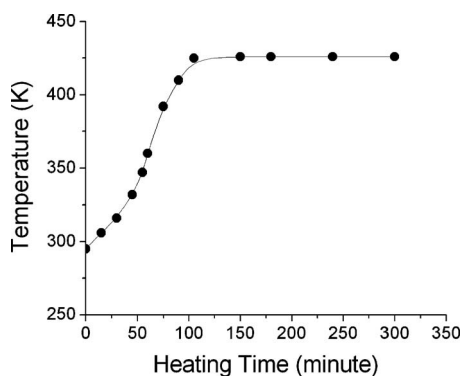


FIG. 3. Temperatures of the vacuum chamber as a function of the heating time at 2100 K.

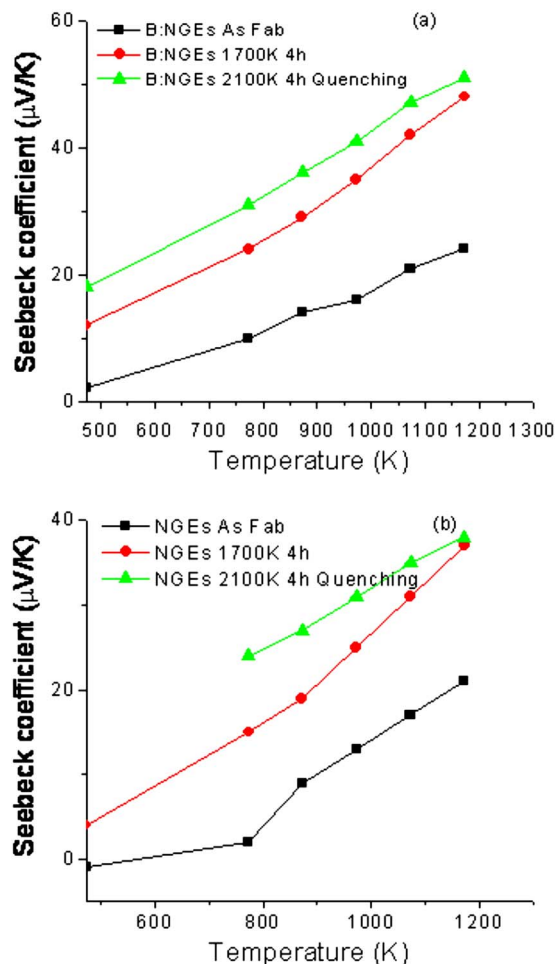


FIG. 4. (Color online) The Seebeck coefficients measured as a function of measuring temperatures for various (a) B:NGEs and (b) NGEs.

F. Effect of quenching on the thermoelectric properties of boron-doped nanocarbon ensembles

We have used the induction furnace for annealing and quenching the boron-doped NGEs (B:NGEs). The samples, are composed of mixtures of nanographite (30 nm, from MTI Corporation) with or without the addition of B_4C (50 nm, from American Elements) powders. These mixtures used ethanol as a binder and were then formed into mechanically rigid compacts by the reaction with methane gas at 1200 K in a chemical-vapor deposition procedure. The final samples had a dimension of $20 \times 10 \times 5$ mm³. The details of the preparation procedures were described in previous paper.⁴ These samples were then placed into the graphite susceptor for annealing and allowed to reach the target temperature in 1 h. The sample was then annealed for 4 h at the target temperature followed by helium gas quenching. Seebeck coefficient and dc electrical conductivity were measured at various temperatures (up to 1200 K) as previously described.⁴

Figure 4 shows Seebeck coefficients for the B:NGEs (NGEs with 5wt % of B_4C powders) and NGEs measured at various temperatures. All the measured data are repeatable within ~10% of deviation. As shown, the Seebeck coefficients increased monotonically with the measuring temperatures up to ~22 $\mu V/K$ in Fig. 4(a) for the as-fabricated

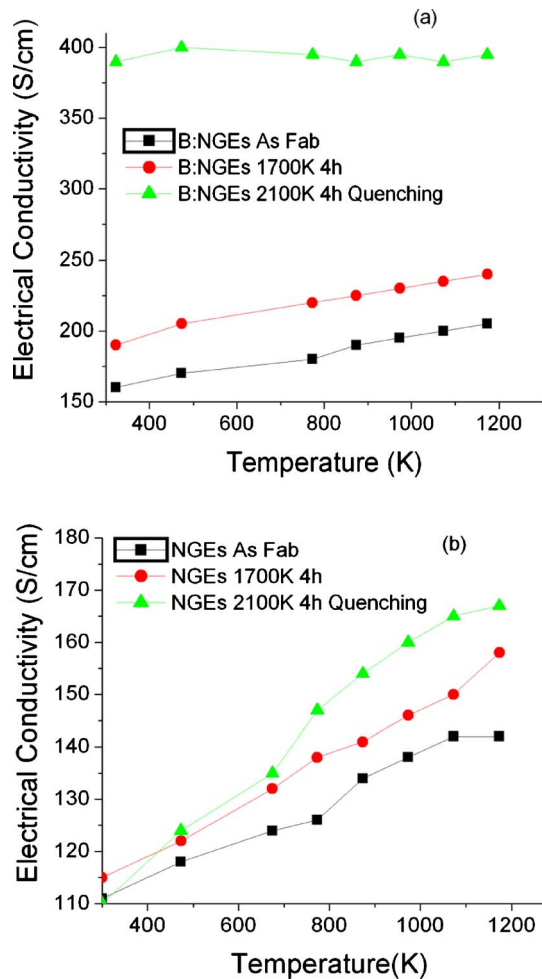


FIG. 5. (Color online) The dc electrical conductivities measured as a function of measuring temperatures for various (a) B:NGEs and (b) NGEs.

B:NGEs, and up to $\sim 20 \mu\text{V}/\text{K}$ in Fig. 4(b) for the as-fabricated NGEs, at 1200 K. Clearly the addition of 5wt % of B_4C powders in the as-fabricated B:NGEs does not enhance the Seebeck coefficients without further annealing. In Fig. 4(a), both of the annealed B:NGE samples show higher overall Seebeck coefficients at all temperatures. Clearly, higher annealing temperatures (2100 K) enhance Seebeck coefficients at all temperatures of measurement. (A maximum value of $\sim 50 \mu\text{V}/\text{K}$ was in fact achieved for samples annealed at 2500 K in a graphite furnace. See Ref. 4.). Similar trends were shown for NGEs annealed at 1700 and 2100 K but the maximum Seebeck coefficient achievable at these temperatures was $\sim 35 \mu\text{V}/\text{K}$. There can be little doubt that boron doping in the B:NGEs is responsible for the observed higher Seebeck coefficients.

We have also measured the electrical conductivities of the B:NGEs and NGEs as shown in Figs. 5(a) and 5(b), respectively. As shown in Fig. 5(a), the dc electrical conductivity of the as-fabricated B:NGEs increases moderately from $\sim 160 \text{ S}/\text{cm}$ at 300 K to $\sim 200 \text{ S}/\text{cm}$ at 1200 K. The dc electrical conductivity of the as-fabricated NGEs increases from ~ 110 to $\sim 150 \text{ S}/\text{cm}$ in the same temperature range as shown in Fig. 5(b). This finding can be interpreted to mean that boron doping enhances the conductivity of as-fabricated NGEs. After annealing at 2100 K, the dc conductivity of

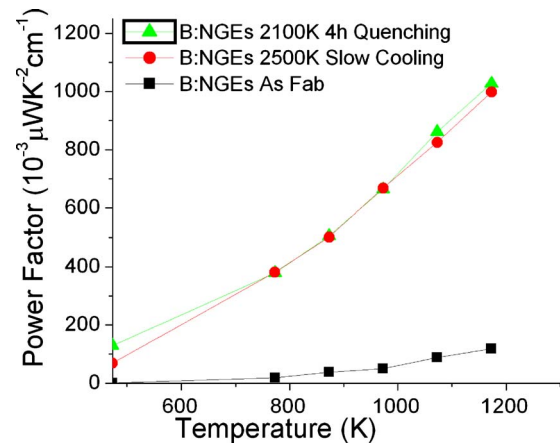


FIG. 6. (Color online) Power factors of various B:NGEs.

B:NGEs and NGEs increased up to $\sim 400 \text{ S}/\text{cm}$ [Fig. 5(a)] and $\sim 170 \text{ S}/\text{cm}$ [Fig. 5(b)], respectively. From Fig. 5(a), annealing of B:NGEs at 1700 K could enhance the conductivity only up to $\sim 240 \text{ S}/\text{cm}$. Apparently, higher annealing temperatures (2100 K) and quenching are responsible for the considerable enhancement of the electrical conductivity of B:NGEs. This enhancement in electric conductivity is not related to the sample packing density as there is no noticeable change in the density ($\sim 1.3\text{--}1.4 \text{ g}/\text{cm}^3$) before and after different heat treatments.

The effect of quenching on the enhancement of Seebeck coefficient and electrical conductivity is illustrated more clearly in Fig. 6 where the power factors ($S^2\sigma$) for B:NGEs measured as a function of temperature for three samples are delineated: (1) the as-fabricated sample, (2) the sample after annealing for 4 h at 2100 K then quenching in a helium atmosphere, and (3) the sample after annealing for 4 h at 2500 K in a resistive graphite furnace and then slow cooling to room temperature. As shown, the power factors for the as-fabricated B:NGEs reach $\sim 100 \mu\text{W K}^{-2} \text{cm}^{-1}$ and are enhanced by about a factor of 10 to $\sim 1000 \mu\text{W K}^{-2} \text{cm}^{-1}$ after annealing at 2100 K by induction heating followed by quenching. The power factors of the quenched B:NGEs are thus comparable to power factors measured on samples that had been annealed at 2500 K and then slow cooled in a graphite resistance furnace. Induction annealing at 2100 K followed by quenching is sufficient for preparing high performance B:NGEs without the need of time consuming annealing at higher temperatures in a graphite furnace. It should be noted that this comparison was performed with different samples fabricated under identical conditions and they displayed very similar as-fabricated thermoelectric properties. The enhancement of thermoelectric properties by virtue of induction annealing and subsequent gas quenching has been convincingly demonstrated in this current set of experiments.

III. SUMMARY

We have designed and fabricated an induction furnace that can achieve 2400 K with helium quenching capability and is highly reliable over prolonged periods of heating. We

estimate that the furnace can be built for less than 1/3 the cost of commercial graphite or induction furnaces. Both Seebeck coefficients and electrical conductivities of boron-doped nanocarbon ensembles increase monotonically temperature after induction annealing followed by quenching. Power factors after 2100 K anneals in the induction furnace followed by quenching are comparable to those obtained by annealing to 2500 K in a graphite furnace followed by slow cooling. The convenience and lower cost of the induction furnace make it a strong contender for carrying out research of the sort described in this paper.

ACKNOWLEDGMENTS

Work supported by the U.S. Department of Energy, BES-Materials Sciences and Engineering, and the EERE Office of Vehicle Technologies under Contract No. DE-AC02-06CH11357. Y.K.Y. acknowledges support from the Argonne National Laboratory (Contract No. 7F-00961, Ming Xie Appointment at ANL from May 2007–May 2010), the U.S. Department of Energy, BES-Materials Sciences and Engineer-

ing (Contract No. DE-FG02-06ER46294), and the National Science Foundation (*CAREER* Grant No. DMR 0447555).

- ¹M. S. Dresselhaus, G. Chen, M. Y. Tang, R. G. Yang, H. Lee, D. Z. Wang, Z. F. Ren, J. P. Fleurial, and P. Gogna, *Adv. Mater.* **19**, 1043 (2007).
- ²X. W. Wang, H. Lee, Y. C. Lan, G. H. Zhu, G. Joshi, D. Z. Wang, J. Yang, A. J. Muto, M. Y. Tang, J. Klatsky, S. Song, M. S. Dresselhaus, G. Chen, and Z. F. Ren, *Appl. Phys. Lett.* **93**, 193121 (2008).
- ³K. F. Hsu, S. Loo, F. Guo, W. Chen, J. S. Dyck, C. Uher, T. Hogan, E. K. Polychroniadis, and M. G. Kanatzidis, *Science* **303**, 818 (2004).
- ⁴D. M. Gruen, P. Bruno, R. Arenal, J. Routbort, D. Singh, and M. Xie, *J. Appl. Phys.* **105**, 073710 (2009).
- ⁵D. L. Carroll, P. Redlich, X. Blase, J. C. Charlier, S. Curran, P. M. Ajayan, S. Roth, and M. Ruhle, *Phys. Rev. Lett.* **81**, 2332 (1998).
- ⁶O. E. Andersson, B. L. V. Prasad, H. Sato, T. Enoki, Y. Hishiyama, Y. Kaburagi, M. Yoshikawa, and S. Bandow, *Phys. Rev. B* **58**, 16387 (1998).
- ⁷D. M. Gruen, P. Bruno, and M. Xie, *Appl. Phys. Lett.* **92**, 143118 (2008).
- ⁸P. C. Redfern, D. Gruen, and L. A. Curtiss, *Chem. Phys. Lett.* **471**, 264 (2009).
- ⁹C. E. Lowell, *J. Am. Ceram. Soc.* **50**, 142 (1967).
- ¹⁰J. C. Matthews, *J. Sci. Instrum.* **34**, 62 (1957).
- ¹¹L. C. F. Blackman, P. H. Dundas, A. W. Moore, and A. R. Ubbelohde, *Br. J. Appl. Phys.* **12**, 377 (1961).
- ¹²A. W. Moore, A. R. Ubbelohde, and D. A. Young, *Br. J. Appl. Phys.* **13**, 393 (1962).
- ¹³P. D. Johnson, *J. Am. Ceram. Soc.* **32**, 316 (1949).